Near Surface Full Waveform Inversion via deep learning for subsurface imaging

A. Parasyris
University Of Strathclyde.
D.Bairaktaris & Associates Ltd.

L. Stankovic
University Of Strathclyde.

S. Pytharouli
University Of Strathclyde.

V. Stankovic
University Of Strathclyde.

ABSTRACT: In order to meet increasing safety standards and technological requirements for underground construction, the estimation of Earth models is needed to characterize the subsurface. This can be achieved via near-surface or standard Full-Waveform Inversion (FWI) velocity model building, which reconstructs the Earth model parameters (compressional and shear wave velocities, density) via recordings obtained on the field. The wave function characterizing the Earth model parameters is inherently non-linear, rendering this optimization problem complex. With advances in computational power, including graphics processing units (GPUs) computing, data driven approaches to solve FWI via Deep Neural Networks (DNN) are increasing in popularity due to its ability to solve the FWI problem accurately. In this paper, we leverage on DNN-based FWI applied to field data, to demonstrate that instead of depending on observed data collected from multiple boreholes across a large distance, it is possible to obtain accurate Earth model parameters for areas with varied geotechnical characteristics by using geotechnical data as prior knowledge and constraining the training models according to a single borehole to map the large geological earth cross section. Also we propose a methodology to simulate acoustic recordings indirectly from laboratory tests on soil samples obtained from boreholes, which were analysed for compressive strength of intact rock and Geological Strength Index. Layers' geometry and properties for a section of total 3.0 km are used for simulating 15 2D elastic spaces of 200 m width and 50m depth assuming receivers and Ricker-wavelet sources. We adopt a Fully Convolutional Neural Network for Velocity Model Building, previously shown to work well with synthetic data, to generate the 2D predicted Earth model. The results of this study show that the velocity model can be accurately predicted via DNN through the appropriate training with minimum demands for borehole data. The performance is evaluated through both metrics focused on image quality and on velocity values giving a multifaceted understanding of the model's true ability to predict the subsurface.

1 INTRODUCTION

Extensive geophysical research is often carried out on large-scale construction projects, such as tunnels, to investigate the complex and changing subsurface. Usual applications may include the estimation of bedrock and groundwater levels, imaging of various subsurface layers, or detection of "weak" material as peat or slide planes (Niederleithinger et al., 2016). Geophysical surveys enable Earth model information (such as velocity of compressional waves V_p, velocity of shear waves V_s and density ρ) to be obtained for large volumes of ground that cannot be investigated by direct methods (McDowell et al., 2002). Specially for tunnel design, in cases when the soil

overburden above the tunnel crown is of great height which means that the required depth of an exploratory borehole will be quite large and so making boreholes will be difficult, the geophysical methods can provide an alternative solution of significant importance. This can be done in addition to the application of the pilot tunnel method where a small-diameter tunnel is constructed, in parallel to the axis of a much larger main tunnel to explore ground conditions, assist final excavation and overcome the difficult ground conditions. Thus, the need for better and stable performance of geophysical methods in subsurface imaging with a limited number of available auxiliary boreholes is a task of great interest in tunnel construction.

The study of the properties of the subsoil is mainly based on the application of seismic methods both for historical and practical reasons since seismic methods use strong natural (earthquakes) or artificial sources (explosions)(K. & V. Papazahos, 2008). The problem that describes the definition of the Earth Model from observed data d (seismic recordings), is finding a non-linear operator G which when applied to the Earth model m (representing the parameters that describe the Earth model e.g., compressional wave velocities, shear wave velocities, density), will produce the observed data d= G(m) (Bogiatzis, 2006). But solving equation for $\hat{m} = G^{-1}d$, that is finding a solution for the Earth Model parameters, is significantly difficult due to the non linear mapping of the wave equation to the measured data and so is often handled through iterative methods. Full waveform inversion (FWI) is a method for solving this problem, that takes advantage from the full shape of the waveform and nowadays is one of the most preferred methods for Velocity Model Building (VMB), that ensure solutions of high accuracy. In recent years, tackling the FWI problem is implemented through deep learning neural network (DNN) architectures and many successful examples can be found in the literature.

Mao et al., (2019), proposed a deep learning-based data assimilation method for tackling VMB which can be considered as similar to the FWI, and they used a convolutional neural network (CNN) in order to predict the prior velocity information with two 2D convolutional layers, four fully connected layers and an activation function that uses hyperbolic tangent (Tanh). The input is a zero – offset seismic gather, the output is the subsurface velocity structure and the presented training dataset is consisted of 5000 synthetic velocity models with 3 to 6 layers of random velocity layers in the range of [2,4] km/s with their corresponding zero-offset gather. They presented test results for a velocity model containing a salt structure.

Zheng et al., (2019), presented two case studies from which the second one was concerning elastic VMB through supervised deep learning approach. They trained a CNN to make predictions of 1D velocity (V_p and V_s) and density profiles. The CNN consists of multiple 2D convolutional layers with 3x3 filter kernels, while between the sets of convolutional layers, a max-pooling layer and a dropout layer are used for downsampling and to control overfitting. They trained their network with 10000 synthetic data while they tested the prediction capabilities of the network on both synthetic and on field data after making simplifying assumptions that the field data present only vertical variation and are horizontally homogeneous.

Li et al., (2020), addressed the mapping of time series to spatial image via the proposed SeismInvNet. The network adopts an encoder-decoder architecture for VMB and tackles the weak spatial correspondence (when a reflected wave exists on the seismic data on a specific position for which the velocity model does not contain an interface and vice versa) and the uncertain reflection – reception relationship between velocity model and seismic data as well as the time varying property of seismic data. The main components of the network are an embedding encoder, a spatially aligned feature generator, a velocity model decoder and a loss function composed by the mean squared error and multiscale structural similarity while the presented experiment consisted of 12000 synthetic training velocity models with their corresponding seismic pairs.

Another implementation is the Fully Convolutional Network named FCNVMB for Velocity Model Building (Yang et al., 2019) which uses a U-Net encoder decoder architecture with skipping layers. The network learns the non linear law between the parameters of the wave equation with training on physical models. In the original paper the authors tested the network for reconstructing Earth Model parameters and in particular P-waves velocity. The 1600 synthetic training models that they used presented salt bodies positioned on constant multilayer velocity background and 130 models from the original Society of Exploration Geophysicists (SEG) model. The encoder is composed by 10 2D convolutional layers while they used a rectified linear unit activation function (RELU). The decoder includes eight 2D convolutional layers connected with the corresponding deconvolutional layers. The authors presented their results in comparison with physics based FWI results for smoothed starting velocity models for two experiments. The first
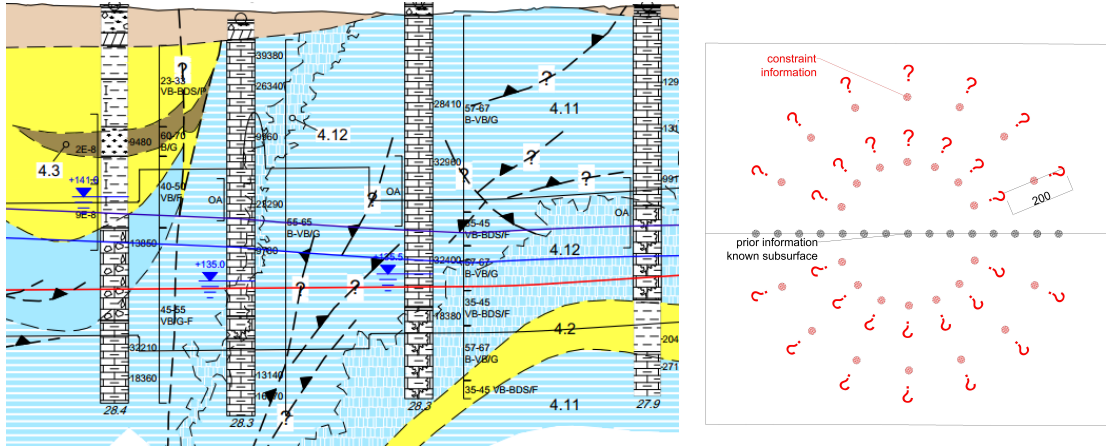
Figure 1. a)Longitudinal Geological Section from field data. Specially for tunnel construction projects, dense boreholes are usually implemented. b)Training velocity models used for the network are generated on known geotechnical area. Subsequently the training velocity models are constrained to single borehole data in every 200m longitudinal distance of the investigated 200m x 50m areas and the new models are added to the initial models forming in total 9000 training models as described in paragraph 2.3.

experiment was on predicting synthetic salt bodies and the second used the pretrained network of the first experiment with addition of 130 SEG models to predict parts of the SEG model.

In this paper we handle the near surface Full waveform Inversion problem through FCN-VMB for reconstruction of the P-waves velocity image of the subsurface with application to field data. All the pairs of velocity and corresponding shot are created through Devito (Louboutin et al., 2019) which is a domain-specific language for implementing high-performance finite difference partial differential equation solvers. The contributions of this paper concern the following: 1)We provide a training methodology for predicting large geological sections based on prior geotechnical knowledge and constraints on sparse density sampling boreholes. 2)We provide a methodology for simulating seismic shots from geotechnical lab data. 3)We present a step by step comprehensive schematic representation of the overall procedure.

2 METHODOLOGY

Here we describe our proposed methodology from generation of acoustic measurements that comprise d, inclusion of elastic displacements to augment the training set, generation of velocity models that comprise m and the experimental setup for the FCNVMB for near surface FWI-VMB to elastic spaces with dimensions 200m width x 50m depth through data obtained from real boreholes of spanning 3.0 km.

2.1 *Borehole data*

As is typical in construction engineering, multiple boreholes are used to collect soil samples across the 3km span. Specialists after laboratory analysis of the collected soil samples, created a subsurface map presenting the space between the boreholes, an example of which is shown in Figure 1a. It indicates the geomaterials that compose each section (claystone, sandstone, siltstone etc.) the main geotechnical characteristic parameters of which, including compressive strength of the intact rock σ_{ci} and the Geological Strength Index GSI can be seen in Tables 1-3. The estimation of the parameters of strength and deformability of the rock mass is of major importance during the design for the opening and support of underground projects. The main difficulty in obtaining these parameters is that the laboratory tests are done on samples of intact rock (without discontinuities) and are therefore not representative for the rock mass which includes discontinuities. Given the uniaxial compressive strength of the intact rock pieces without discontinuities σ_{ci} and the Geological Strength Index GSI, the modulus of elasticity of the rock mass is calculated according
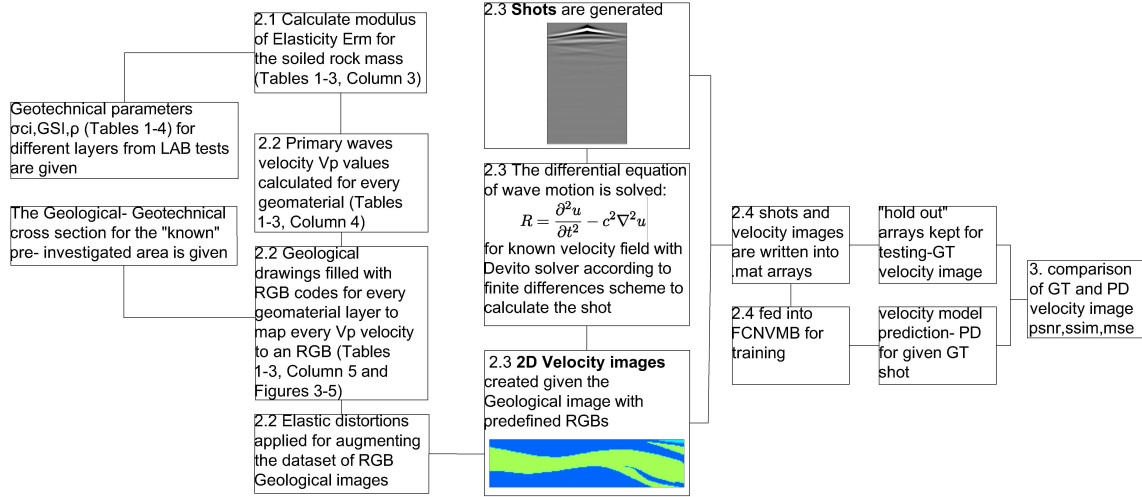
2.1 Calculate modulus of Elasticity Erm for the soiled rock mass (Tables 1-3, Column 3)

2.3 **Shots** are generated

Geotechnical parameters σci,GSI,ρ (Tables 1-4) for different layers from LAB tests are given

2.2 Primary waves velocity Vp values calculated for every geomaterial (Tables 1-3, Column 4)

The Geological- Geotechnical cross section for the "known" pre- investigated area is given

2.2 Geological drawings filled with RGB codes for every geomaterial layer to map every Vp velocity to an RGB (Tables 1-3, Column 5 and Figures 3-5)

2.3 The differential equation of wave motion is solved:

$$R = \frac{\partial^2 u}{\partial t^2} - c^2 \nabla^2 u$$

for known velocity field with Devito solver according to finite differences scheme to calculate the shot

2.4 shots and velocity images are written into .mat arrays

"hold out" arrays kept for testing-GT velocity image

3. comparison of GT and PD velocity image psnr,ssim,mse

2.4 fed into FCNVMB for training

velocity model prediction- PD for given GT shot

2.2 Elastic distortions applied for augmenting the dataset of RGB Geological images

2.3 **2D Velocity images** created given the Geological image with predefined RGBs

Figure 2.   Schematic representation of the proposed Methodology.

to the following equation which is proposed by Hoek et al.,(1997), and is a modification of the empirical relationship of Serafim and Pereira,(1983):

$$E_{rm} = \sqrt{\sigma_{ci}/100} * 10^{(GSI-10)/40} \tag{1}$$

Where: σ_{ci} is the compressive strength of the intact rock in MPa, GSI is the Geological Strength Index and E_{rm} in the elastic modulus of deformation of the rock mass in GPa. These are listed in Tables 1-3 for three sections. Sections A and B span 1.2km each and Section C spans 0.6km. For simplification, the mean and standard deviation of the densities are used for modelling - these are shown in Table 4.

2.2   *Calculation of the Acoustic Velocities from Geotechnical Laboratory Data with Inclusion of Elastic Displacements*

The acoustic velocity is calculated as $V_p = \sqrt{(E_{rm}/\rho)}$, where E_{rm} is the modulus of elasticity of the rock mass for each layer and ρ the density for every section (Table 4). V_p is shown in Tables 1-3 (Column 4) which is mapped to a unique Red-Green-Blue (RGB) code shown in Tables 1-3 (Column 5), for every geomaterial in every geological section A,B or C, which after is assigned to every subsurface layer in the initial drawing created by specialists. The generated images presented in Figures 3,4,5 are then resized in order to correct the drawing scale and to represent the physical analogy of the elastic space studied (200m x 50m). After the calculation of the velocity model and the extraction of the RGB image files, elastic displacements are added to the images in order augment the training dataset, to strengthen the generalization of the network and to avoid overfitting (Bloice et al., 2017). In our dataset, a Gaussian Distribution is used for sampling distortion on the center of the image, through the gaussian distortion function with parameters grid width=3, grid height= 3,magnitude= 90 and corner=bell.

2.3   *Creation of the Velocity Models and Calculation of the corresponding shot for input to deep learning FWI network*

The total length of the geotechnical sections is 3.0 km and the length of every elactic space for the modelling of the wave equation in Devito has a physical size with dimensions (201.,51.) and grid spacing (1.,1.). Two experiments have been implemented in this paper each one containing 9000 models: 1)Experiment 1 at which 9000 training velocity models are generated for the "known subsurface area" which then are used to predict "unknown subsurface areas" and 2)Experiment 2 at which the 9000 training models are generated for the "known subsurface area" but part of them (4800/9000) is constrained to velocity values obtained from a single borehole data in the "unknown subsurface areas". Also a number a small number of subsection images (1800/9000) is taken from the "known subsurface area" for every geological section and used in the training set. Subsequently the generated images are used to generate velocity arrays for the target RGBs

Table 1.   Geotechnical Properties of Section A

Geomaterial category	$\sigma_{ci}(Mpa)$	GSI	$E_{rm}(Mpa)$	$V_p(m/s)$	$*RGB$
Claystone, Calcareous claystone	7.60	29	822	588	(150,150,150)
Sandstone, Calcareous sandstone	14.25	43	2487	1022	(0,255,255)
Breccia, Calcareous Breccia	17.10	55	5397	1506	(255,255,255)
Sandstone-calc.sandstone with	-	-	-	-	-
claystone-calc. claystone intercalations	8.55	35	1244	723	(0,255,0)
Siltstone and sandstone alternations	9.03	35	1243	723	(0,0,0)
Marly limestone	20.90	42	2851	1095	(0,0,255)
Thin bedded marly limestone	20.90	51	4927	1439	(255,0,255)
Karstic marly limestone	20.90	47	3748	1255	(255,255,0)
Limestone	28.50	67	14184	2441	(255,0,0)

*RGB codes shown in section A shown in Figure 3.

Table 2.   Geotechnical Properties of Section B

Geomaterial category	$\sigma_{ci}(Mpa)$	GSI	$Erm(Mpa)$	$V_p(m/s)$	$*RGB$
Claystone, Calcareous claystone	7.60	38	1382	762	(75,75,75)
Sandstone, Calcareous sandstone	14.25	45	2774	1080	(150,150,0)
Breccia, Calcareous Breccia	17.10	49	3995	1296	(125,125,125)
Claystone -calc. claystone	-	-	-	-	-
with sandstone intercalations	9.03	32	1084	675	(0,125,0)
Siltstone and limestone intercalations	14.73	29	1176	703	(0,0,20)
Sandstone-calc.sandstone with	-	-	-	-	-
claystone-calc. claystone intercalations	8.55	40	1635	829	(0,0,125)
Siltstone and sandstone alternations	9.03	37	1426	774	(125,0,125)
Calcareous marl	12.35	48	3214	1162	(132,132,132)
Marly limestone	20.90	56	6476	1650	(125,0,0)
Thin bedded marly limestone	20.90	60	8060	1840	(255,255,255)
Limestone	28.50	55	7160	1734	(5,5,0)

*RGB codes shown in section B shown in Figure 4.

Table 3.   Geotechnical Properties of Section C

Geomaterial category	$\sigma_{ci}(Mpa)$	GSI	$E_{rm}(Mpa)$	$V_p(m/s)$	$*RGB$
Limestone	38.00	57	9223	1962	(150,150,150)
Claystone, Calcareous claystone	7.60	42	1720	847	(75,75,75)
Sandstone, Calcareous sandstone	14.25	36	1696	841	(150,150,0)
Breccia, Calcareous Breccia	17.10	48	3581	1223	(125,125,125)
Claystone -calc. claystone	-	-	-	-	-
with sandstone intercalations	9.03	36	1313	740	(0,125,0)
Siltstone and sandstone alternations	9.03	27	781	571	(125,0,125)
Marly limestone	20.90	15200	51	1415	(125,0,0)
Thin bedded marly limestone	20.90	49	4297	1340	(255,255,255)
Karstic marly limestone	20.90	38	2355	992	(255,255,0)
Limestone	28.50	61	10216	2065	(5,5,0)

*RGB codes shown in section C shown in Figure 5.

Table 4.   Density used for modelling various section layers

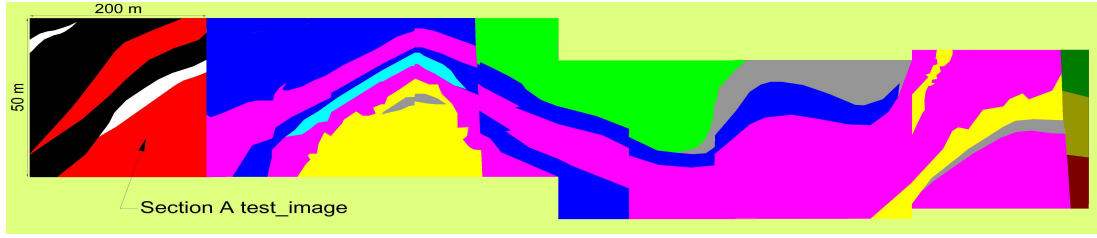| Section	$\rho_{mean}(kg/m^3)$	$std(kg/m^3)$
Geomaterials of Section A	2380	79.06
Geomaterials of Section B	2380	87.65
Geomaterials of Section C	2395	98.46

Figure 3.   Geotechnical section A, with total length of 1.2 km. The arrow shows the "TEST- Ground Truth" image for this section.
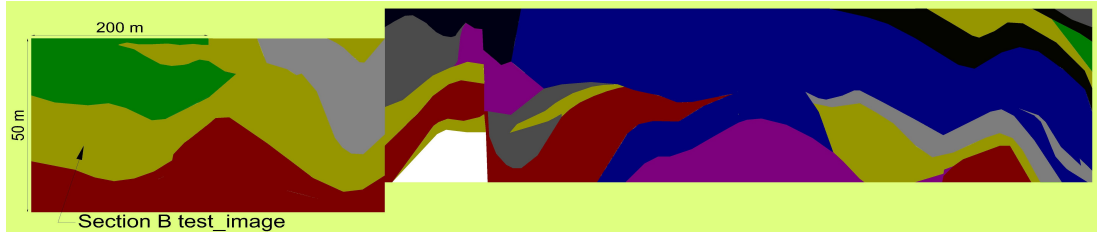

Figure 4.   Geotechnical section B, with total length of 1.2 km. The arrow shows the "TEST- Ground Truth" image for this section.
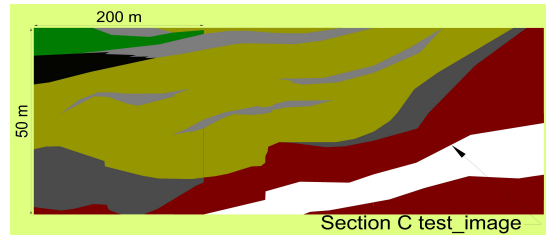

Figure 5.   Geotechnical section C, with total length of 600 m. The arrow shows the "TEST- Ground Truth" image for this section.

according to the mapping shown in Tables 1-3. Then, the calculation of the pair seismic shots that are used for the training of the network is implemented from the solution of the constant density acoustic 2D wave equation in the time domain according to the finite differences method which is defined as $R = \frac{\partial^2 u}{\partial t^2} - c^2 \nabla^2 u$, where u is the displacement field, c is the p wave velocity field and R is the Ricker source propagator.

The wave equation is solved for a Ricker Source at depth of 1 m with a peak frequency of 0.010 KHz, receivers placed every 1m, at depth of 1m and the simulation lasted 2000 milliseconds. In this study we have assumed a single source in order to aim at low costs, although the total number of receivers could also be important. So we have assumed a very dense in-line arrangement of surface receivers in the simulations in order to transfer to the network a greater amount of information from the seismic recordings. The in-line spacing between receivers could be optimised accordingly in order to lead to a more realistic placement.

2.4   *DNN-based FWI setup*

When the solution of the differential equation is completed the velocities and the corresponding displacements are stored in arrays with dimensions 2000x200 for the displacements in the x-t domain and 50x200 for the velocities in the x-z domain, and are written into two separate Matlab files (.mat) and then passed to the FCNVMB for the training and testing procedures. The training/testing ratio used in the process is 9000:2250 for both experiments 1 and 2. The number of the epochs is set to be 100, the test batch size equal to 10 and the learning rate used is set to be equal to 1e-3. The training process lasted 8.50 hours on a GPU NVIDIA RTX A4000 while the testing process took a couple of minutes.

3 EXPERIMENTAL RESULTS

In all velocity images that can be seen in Figure 6, the horizontal axis shows the width in kilometers and the vertical axis the depth in kilometers, while the maximum depth is shown at the zero 0.00 km level. Velocity has units of km/s. Finally in the velocity profile diagram the velocity is in m/s units while the maximum depth is at the 50.00 m level of the vertical axis. Experiment 1 is shown in column 1, experiment 2 at column2 and ground truth (GT) at column 3.

3.1 *Quantitative comparison of results in terms of image metrics psnr and ssim*

The peak signal to noise ratio (psnr) is a quality image metric that the higher it is, the better the quality of the image being considered. The psnr between the prediction of the network trained on the experiment 2 and ground truth image is improved by 11.42 % compared to the prediction of the trained on the experiment 1 and ground truth for section A (Figure 6,1st row), 4.5 % for section B (Figure 6,2nd row) and 27.75 % for section C (Figure 6,3rd row). The structural similarity index (ssim) from the other hand is a quality metric used to measure how similar two images are, based on loss of correlation, luminance distortion and contrast distortion. For the case of experiment 2 ssim is calculated to be 3.11 %, 1.11 % and 0.9 % greater than the ssim calculated for the experiment 1. More specifically the (psnr,ssim) values for the 2nd dataset are (16.00,0.928),(23.75,0.984) and (30.07,0.99) for sections A B and C respectively which can be considered as high values.

3.2 *Quantitative comparison of results in terms of metrics applied on velocity values, mse*

The extracted values for the ground truth, and the predictions for both experiments are plotted for a vertical cut in the middle (at 100m position)of the elastic space and can be seen in Figure 6 (column d). The mean squared error (mse) for experiment 1 regarding to the three sections A,B,C is 2.01,3.77 and 5.38 greater compared to the mean squared error calculated for experiment 2.

3.3 *Qualitative comparison of results*

As we can observe in Figure 6, 1st row, we have a complete prediction of the velocities for the case of the experiment 2 (2nd column) training. There is some weakness in the prediction of the thickness of the geological layers and in the shape of the geological layers. This is also reflected as a lag in the vertical one-dimensional velocity profile in which we see that the prediction reaches the correct estimated value but little later for the specific GT image. For the case of experiment 1 the predicted image (column 1) does not capture neither the geometry neither the correct velocity range of the GT image. The only successful point in the prediction is the first meters of the velocity image where the network correctly predicts low velocity values, but incorrectly maintains them at greater depths. It is worth at this point to comment on the fact that in this example the mse difference between the two datasets (2.01 % with respect to the values of the velocity profile) is much smaller compared to the next two images not because the network approaches the correct value but because the delay in estimating the correct velocity from the 2nd dataset also leads to a very large mse error calculation which is not quite representative for this specific case since the prediction is quite good. In Figure 6, 2nd row, we see the successful prediction after training on 2 experiment and unlike before we do not notice the same degree of failure in the prediction of the layer thickness. This is also reflected in the vertical profile where all branches except the third are in perfect coincidence. On the contrary, the prediction concerning the experiment 1 fails to capture the gradation of bottom velocities so good. In Figure 6, 3rd row, we see the successful prediction after training on experiment 2 as opposed to the prediction after training on experiment 1 where it completely fails to predict the velocity of the upper levels. This failure is what levels up the mse since it involves many pairs of velocity values. Also as we see at greater depths the network incorrectly predicts some low velocity values that do not exist.
Constraining the training dataset to velocity values obtained from just a single borehole data in combination with the use of subsection images in parallel with application of elastic displacements can strengthen the prediction ability of the network and lead to successful results on field data.
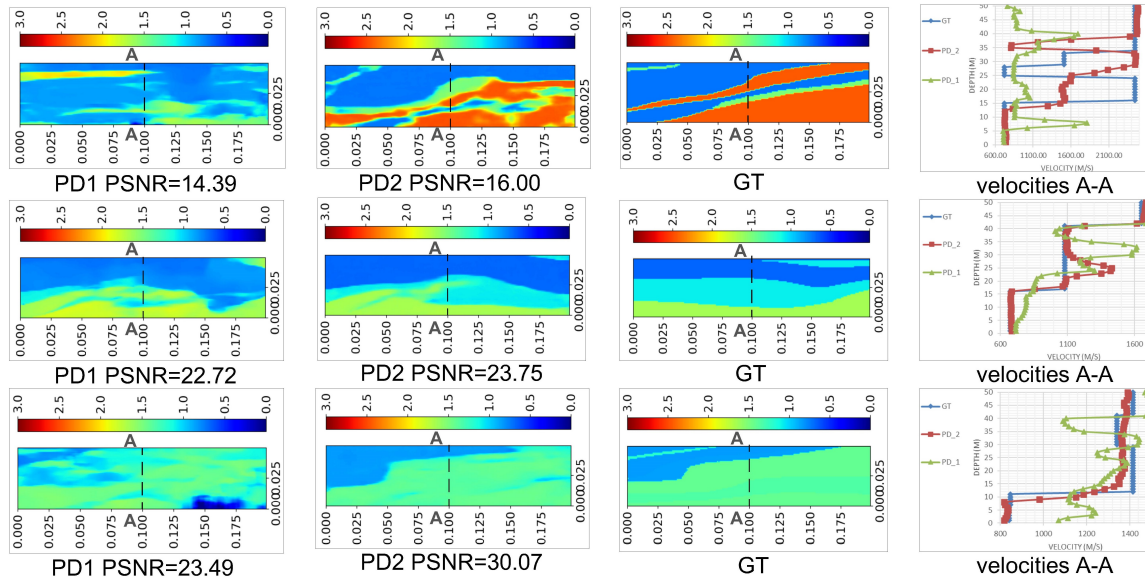
Figure 6. Reconstructed Velocity Models. Geotechnical Sections: A-1st row,B-2nd row and C-3rd row, Experiments: (column a) prediction 1, (column b) prediction 2, (column c) ground truth, (column d) middle-vertical 1D velocity profile from which mse of velocities is calculated.

3.4 *Conclusions*

The results directly show that the proposed method can lead to great performances over field data. Especially for tunnel construction in cases when the soil overburden above the tunnel crown is of great height and in general when making sampling boreholes is difficult, DNN-FWI can predict for the unknown subsurface based on a very limited- sparse number of auxiliary boreholes.

REFERENCES

[1]A. Adler, M. Araya – Polo and T. Poggio," Deep Learning for Seismic Inverse Problems", IEEE Signal Processing Magazine, IEEE, 2021.

[2]B. Mao, L.G. Han, Q. Feng, Y.C. Yin," Subsurface velocity inversion from deep learning-based data assimilation", Journal of Applied Geophysics, Elsevier, 2019.

[3]E. Hoek, E.T. Brown, "Practical estimates of rock mass strength", Int. Journal of Rock Mech. and Min. Sciences, Elsevier, 1997.

[4]E. Niederleithinger, O. Abraham, M. Mooney, "Geophysical Methods in Civil Engineering: Overview and New Concepts ", Int. Symposium Non-Destructive Testing in Civ. Engineering, Berlin, 2016.

[5]F. Yang and J. Ma, "Deep learning inversion: a next generation seismic velocity-model building method", Geophysics, SEG, 2019.

[6]J.L. Serafim, and J.P. Pereira, "Considerations on the Geomechanical Classification of Bieniawski", Proceedings of Int. Symposium on Engineering Geology and Underground Openings, Portugal, 1983.

[7]K. and V. Papazahos," Introduction to Geophysics", ZHTH, 2008.

[8]M. Louboutin, M. Lange, F. Luporini, N. Kukreja, P. A.Witte, F.J.Herrmann, P.Velesko and G. J.Gorman, "Devito v.3.1.0: an embedded domain – specific language for finite differences and geophysical exploration", Geoscientific Model Development, Copernicus Publications, 2019.

[9]M.D. Bloice, C. Stocker, A. Holzinger, "Augmentor: An Image Augmentation Library for Machine Learning",The Journal of Open Source Software, 2017.

[10]P. Bogiatzis,"Two-Dimensional Inversion of Seismic Diffraction Tomography Data", Phd Diss., 2006.

[11]P. W. McDowell, R. D. Barker, A. P. Butcher, M. G. Culshaw, P. D. Jackson, D. M. McCann, B. O. Skipp, S. L. Matthews, J. C. R. Arthur J. C. R.," Geophysics in Engineering Investigations", Construction Industry Research and Information Association ,2002.

[12]S. Li, B. Liu, Y. Ren, Y. Chen, S. Yang, Y. Wang," Deep-Learning Inversion of Seismic Data", IEEE Transactions On Geoscience And Remote Sensing, IEEE, 2020.

[13]Y. Zheng, Q. Zhang, A. Yusifov, Y. Shi," Applications of supervised deep learning for seismic interpretation and inversion", The Leading Edge, 2019.